Check for updates

Precision Silicon Exfoliation Tool Design

Martin J. Ward[1]
Department of Mechanical Engineering,
University of Texas at Austin,
Austin, TX 78705
e-mail: mjward@utexas.edu

Dipankar Behera
Department of Mechanical Engineering,
University of Texas at Austin,
Austin, TX 78705
e-mail: dipankar.behera@utexas.edu

Michael A. Cullinan
Department of Mechanical Engineering,
University of Texas at Austin,
Austin, TX 78705
e-mail: michael.cullinan@austin.utexas.edu

The desire for thin-film silicon is motivated by the growing needs for flexible electronics, compact packaging, and advanced solar power. In previous work we have presented exfoliation as means to a cost effective way to achieve thin-film silicon and described an open loop prototype exfoliation tool that could be used to produce improved films compared to previous methods. However, controllable film thickness, film uniformity, and surface roughness were all challenges with the open loop setup. This paper describes the design, construction, and testing of an improved controlled exfoliation tool with load compensation and inline metrology for closed loop control of the exfoliation process. The exfoliation performance results are compared to those from the proof-of-concept tool and show 53% improvement in silicon uniformity and 67% improvement in average surface roughness. These improvements can be attributed to the addition of load compensation and the improvement in the precision motion of the stage, respectively.
[DOI: 10.1115/1.4055320]

Keywords: advanced materials and processing, metrology, nontraditional manufacturing processes

1 Introduction

The constant demand for miniaturized portable electronics capable of storing, processing, and communicating copious amounts of data has enabled the growth of the semiconductor industry. Since the days of the first integrated chip, the complexity of semiconductor processing and integration steps has grown exponentially, while the cost has gone down due to high production yields and robust supply chains. This has introduced novel microscale integrated systems with applications in state-of-art smartphones, aerospace and automotive sensors, biomedical devices, internet-of-things (IoT) devices, and health monitoring technologies. As we transition into the next phase of integrated devices, flexible and wearable electronics are gaining popularity due to their compactness, conformity, lightweight, and bio-compatibility [1]. Using novel materials and fabrication methods, flexible electronics have proposed applications in wearables [2,3], consumer electronics displays [4], biosensors [5], health diagnostics [6], soft robotics [7], energy harvesting devices (rollable solar cells) [8–11], and structural health monitoring [12].

The concept of flexible electronics has persisted for several decades, but their real potential and practical applications have gained traction after significant advances in new materials like graphene, conductive metallic and polymer inks, liquid metals, and carbon nanotubes [1,13]. By definition, flexible electronics must reliably maintain device performance while undergoing several cycles of large deformations in the form of bending, stretching, twisting, and conforming to irregular topologies like skin or clothing [14]. In addition to these mechanical requirements, the substrate materials for flexible electronics must also be compatible with existing CMOS manufacturing techniques, novel fabrication and integration techniques, and flexible electronics architectures for robust device performance. Unlike organic materials, silicon meets all these requirements.

Thin film monocrystalline silicon can be fabricated using several different processes like thinning of the backside of the wafer using chemical mechanical polishing (CMP) [15], ion implantation [16], etching, and exfoliation (or spalling [17]). CMP involves uniform removal of more than 90% of the wafer's back surface, so it is difficult to process and handle the wafer with the device layers intact. CMP may also introduce microscale defects during the thinning process which can lead to rupturing. Additionally, the process is slow and cost prohibitive. Ion implantation can significantly damage the device layer, and therefore cannot be implemented on a prefabricated wafer.

Surface texturing using dry and wet etch combined with wafer thinning addresses the key issue of reliably achieving better strength in thin monocrystalline silicon. Kashyap et al. demonstrated 60 μm thick rollable monocrystalline films with $2\times$ higher bending strength and 43% lower radii of curvature with intact or better device performance [18]. The nanoscale features in silicon effectively reduce the effect of randomly distributed micro-defects using the stress shielding effect, thereby improving the overall strength after thinning.

Exfoliation is the process of propagating a crack just beneath the surface of a substrate, driven by stress concentrations created by a tensile layer adhered on top of the substrate [17]. The phenomenon of exfoliation is an extension of the failure modes often seen in brittle materials where the presence of coatings with dissimilar thermomechanical properties undergoing thermal stresses leads to substrate fracture [19]. Exfoliation is an interesting method for producing flexible thin film monocrystalline silicon because it is fast and cost effective. However, exfoliation often suffers from poor thickness control and uniformity. Therefore, there is a need for a better, more controlled exfoliation process to obtaining monocrystalline thin silicon films for applications in wearable electronics.

There are several different approaches that have been explored for large area exfoliation of thin silicon films. Some of the initial work on exfoliation was uncontrolled/spontaneous propagation of a crack to achieve thin film silicon for high power-to-weight solar cell applications. The process of spontaneous exfoliation involves bonding silicon with a material with a different coefficients of thermal expansion (CTE) and heating the sample to induce stress. Due to the mismatch in CTE, a fracture is spontaneously initiated in the silicon and cracks propagate on multiple fronts. This leads to poor surface roughness and uniformity, which are undesirable for high performance devices. Hensen et al. demonstrated directional heating and cooling cycles for controlled exfoliation, but the layer thicknesses obtained from this approach were still between 50 and 80 μm [20]. An exfoliation method developed by Applied Novel Devices Inc., a spin-off from the University of Texas at Austin used a wedge tool to propagate the crack by applying a prying load [21]. In this method, a nickel tensile layer is electroplated on a nickel seed layer evaporated on top of an adhesion layer. After heat treatment and cooling, residual thermal stresses develop in the nickel layer. Next, a wedge is used to control the crack propagation energy and direction. However, this approach

[1]Corresponding author.

Contributed by of ASME for publication in the Journal of Manufacturing Science and Engineering. Manuscript received February 27, 2022; final manuscript received August 16, 2022; published online September 27, 2022. Assoc. Editor: Satish Bukkapatnam.

Copyright © 2022 by ASME

://asmedigitalcollection.asme.org/manufacturingscience/article-pdf/145/2/024501/6919480/manu_145_2_024501.pdf?casa_token=Rj5vsSdcsGUAAAAA:VzmV6JDaYR6fdRjDFGw7A4JUq2PUpl6WlFnVsUSqRbvklgI7lhOhvFSrhBdRF2DSEISKcgU by University of Texas At Austin user on 07 S

does not constrain the force at all, and applies only a displacement condition to the film, thereby introducing friction and stick/slip conditions which can lead to poor surface roughness and non-uniform film thicknesses.

A different approach was taken by Bedell et al. at IBM who sputtered a nickel tensile layer instead of electroplating it [17,22]. Sputtering improved the consistency of the tensile layer and introduced residual stresses without the need for an additional thermal step. Then, an adhesive handle layer of polyimide tape was placed on top of the nickel layer and manually peeled off to get the exfoliated film. However, manual control of the crack propagation direction and an unconstrained film create similar problems as the previous exfoliation methods [17,22].

Previous work by Ward and Cullinan [23] introduced a novel prototype for thin-film exfoliation, which used a model to inform the tool's design [24]. A prototype tool for controlled exfoliation of monocrystalline films was introduced which combined the concept of controlling the exfoliation rate as explored by Applied Novel Devices using the wedge tool and the handle layer concept demonstrated by Bedell et al. [17] for better control over the exfoliation process. Although the prototype results were promising, they also highlighted areas that could be improved to create thinner and more uniform silicon films. The new version of the tool that is presented in this paper has improved precision motion and gathers data from inline metrology to calculate the compensated load curves using the inverted metamodel. We will show that this closed loop control of the exfoliation process helps to significantly improve the thickness accuracy, thickness uniformity, and surface roughness of the exfoliated thin films and make the exfoliation process more robust to variations in the tensile layer.

2 Precision Tool Design

Results from the previous tool and model indicated that undesirable variation in the silicon thickness was largely due to uncontrollable variation in the nickel tensile layer. The model developed with the previous tool also indicated that these variations could be compensated for if they could be measured before exfoliation. To achieve this compensation a new tool design was required. The new tool's motion must be precise enough to measure the variation in the nickel tensile layer with enough accuracy to correctly compensate for it. Then a new mechanism must be incorporated to actively apply the compensating load through the handle film while not damaging the surface roughness of the exfoliated wafer.

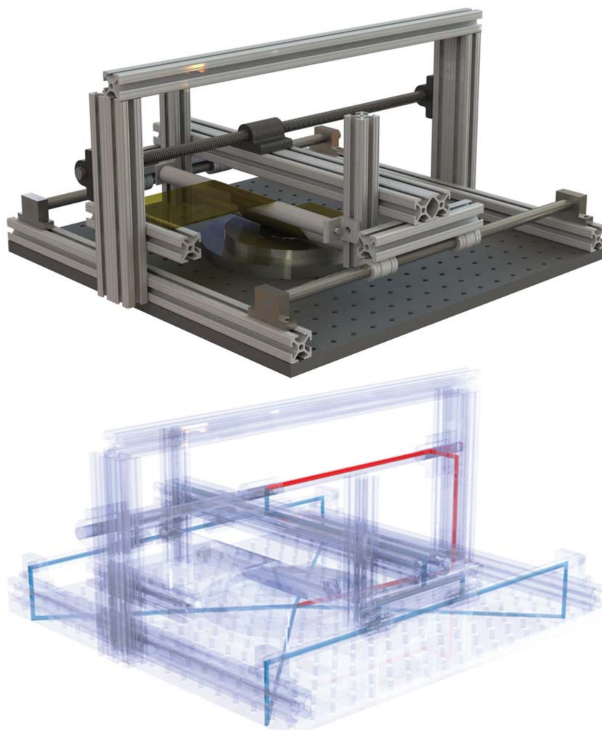

Fig. 1 HTM for prototype tool showing the load path between the leadscrew actuator, through the exfoliation frame, to the vacuum chuck

2.1 Homogeneous Transform Matrix Analysis.

The desired accuracy of less than 0.5 μm for measuring film thickness necessitated a redesign of the stage. Under the off-axis actuation load, the previous prototype demonstrated errors of approximately $\pm$5 μm in the vertical axis. The model developed in a previous work [24] indicated that the exfoliation process was not sensitive in this dimension. Although the stage bushing clearance was helpful in aiding the rapid fabrication and testing of the first prototype, it is not acceptable when incorporating inline metrology. To improve the stage performance, a precision machine design analysis was performed on the system and homogeneous transform matrix (HTM) models of the exfoliation and metrology loops were constructed. The primary source of error was identified as excessive clearance in the four stage bushings.

The analysis indicated that error could be reduced by both replacing the bushings with low-clearance bushings in a housing with increased rigidity and increasing the shaft diameter. In response to the increased stiffness of this configuration, one set of bushings was flexure mounted to avoid over-constraining the system. The bushings were chosen over ball bearing linear guides to promote damping and reduce vibrations that could affect the surface finish of the silicon film. Air bearings were also considered, but ruled out due to a lack of stiffness and benefits compared to cost. It was also noted that the off-axis leadscrew actuator (visible in Fig. 1) was causing an undesirable moment load that was exacerbating the bushing deflection. In response, the actuator was moved to be in line with the stage rails and wafer, as seen in Fig. 2.

3 Load Compensation

The goal of the tool improvements was to remove the overall curvature from the silicon film, shown in Fig. 4 and to minimize the silicon film thickness. To accomplish load compensation, it was necessary to design and implement a control system that could incorporate an inverse form of the metamodel developed in our previous work and process the sensor data collected on the new tool (Fig. 3). Active tension control, pictured in Fig. 2, was added to the tool. The system uses a pair of Airpel Anti-Stiction pneumatic cylinders to create a balanced load across the film. The cylinders are mounted on a load cell and share the same input pressure controlled by a ControlAir 900X E/P transducer. The transducer input is controlled by a National Instruments myRIO running a PID loop with the load cell output as the control variable. With this controller, the system can maintain constant handle film tension to within $\pm$10 mN during exfoliation. This system can also be used to input a specific tension force profile to generate a desired silicon film thickness. Combined with the metamodel and inline metrology, this feature creates the ability to compensate for errors in the electroplated nickel thickness and drive the silicon film thickness to a minimum that is uniform across the wafer.

The first step for creating the compensated load profile is to reconfigure the model from previous work [24] to take an input of desired uniform silicon thickness and output a tension profile. This was done using a Gaussian process regression package [25,26] in PYTHON to create an inverted form of the previous metamodel that predicts handle tension instead of silicon film thickness. This is a more general and faster method than used in previously and the details of the implementation can be seen here [27]. The measured nickel thickness and stress profiles are then input to the model, along with the desired silicon film thickness, and the calculated load profile is produced and uploaded to the tool.

Downloaded from http://asmedigitalcollection.asme.org/manufacturingscience/article-pdf/145/2/024501/6919480/manu_145_2_024501.pdf?casa_token=Rj5vsSdcsGUAAAAA:VzmV6JDaYR6fdRjDFGw7A4JUq2PUpl6WlFnVsUSqRbvklgI7lhOhvFSrhBdRF2DSEISKcgU by University of Texas At Austin user on 07 S

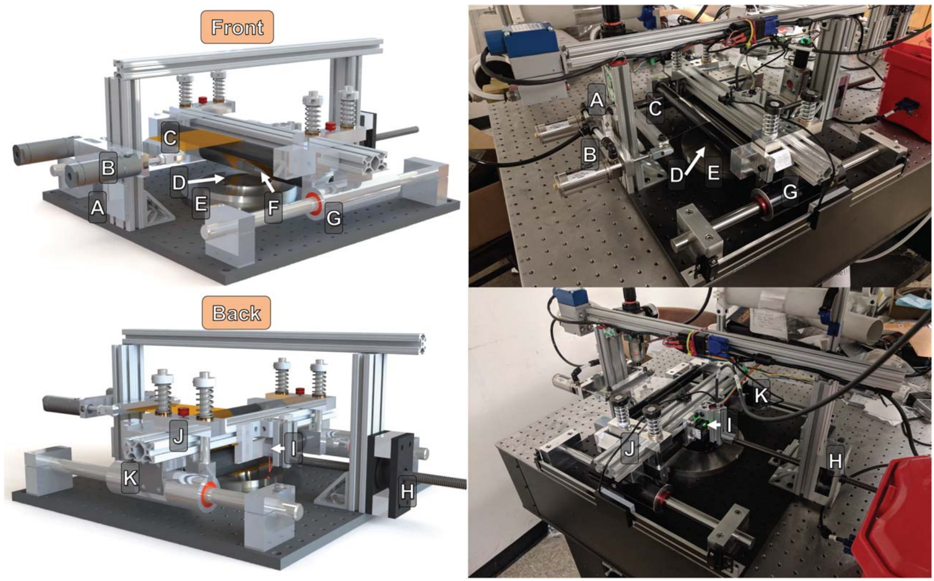

Fig. 2 Render of enhanced exfoliation tool including laser distance sensor and improved motion stage showing: A, load cell; B, pneumatic tensioner; C, handle film; D, silicon wafer; E, vacuum chuck; F, exfoliated film; G, bushing assembly; H, actuator; I, laser distance sensor; J, roller height adjustment; and K, flexure mount

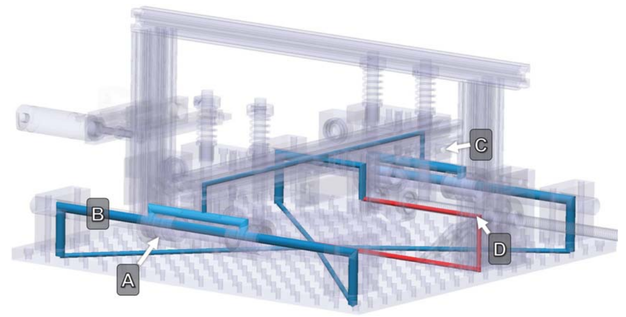

Fig. 3 HTM load path for precision roller tool with active compensation. Key improvements: A, low-clearance bearings; B, larger rails; C, flexure mount; and D, aligned actuator

4 Inline Metrology

The metrology methods used to create the model in previous work [24] and described in [28] were slow, cumbersome, and required that the wafer be transported between multiple metrology tools between each step of the exfoliation process. Incorporating the means to measure the thickness and stress of the wafer in the tool itself greatly simplifies the process required to predict the exfoliated film thickness. With the prediction information, a compensated load profile can be created that allows the tool to create uniform films from nonuniform initial conditions in the nickel thickness and stress.

The measurements were taken with a Micro-Epsilon optoNCDT 1420 laser displacement sensor mounted to the stage as seen in Fig. 2. The sensor was chosen for its high accuracy, compactness, and availability. Manufacture reports stated that it was compatible

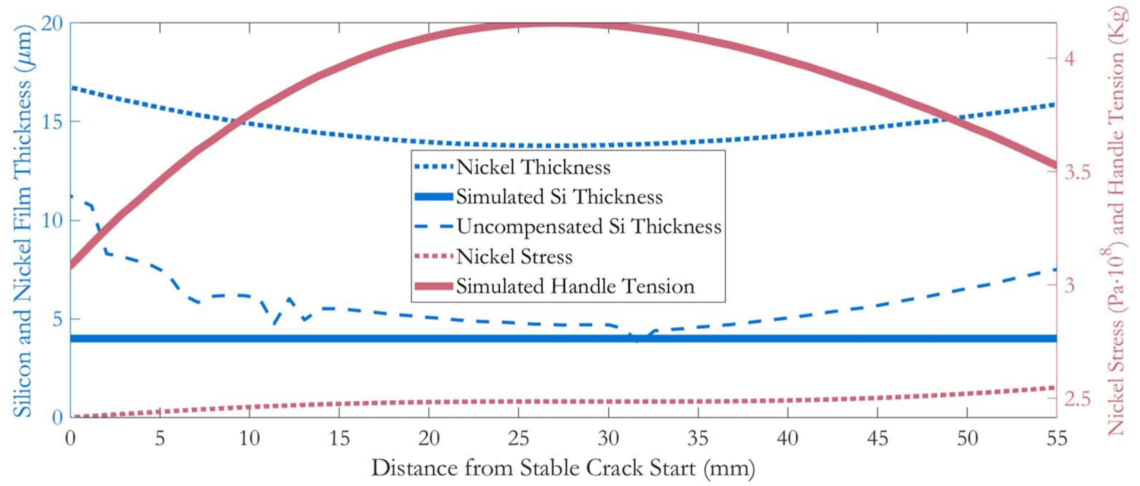

Fig. 4 Simulation of compensated load calculation from previous measurements. Silicon and nickel thickness profiles are shown on the left axis and nickel stress and handle film tension on the right.

Downloaded from http://asmedigitalcollection.asme.org/manufacturingscience/article-pdf/145/2/024501/6919480/manu_145_2_024501.pdf?casa_token=Rj5vsSdcsGUAAAAA:VzmV6JDaYR6fdRjDFGw7A4JUq2PUpl6WlFnVsUSqRbvklgI7lhOhvFSrhBdRF2DSElSKcgU by University of Texas At Austin user on 07 S

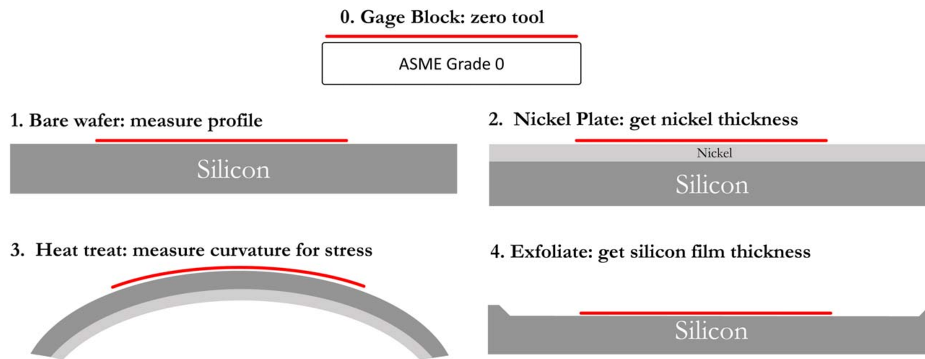

Fig. 5 Inline metrology process flow. The lines above indicate laser measurement location.

with spectral surfaces like silicon wafers, but some diffusing layer had to be applied to get a signal on fully spectral surfaces. Ideally this sensor could be replaced with a confocal probe. To obtain measurements for the nickel thickness and stress and exfoliated silicon thickness, a series of scans were performed in the order shown in Fig. 5.

5 Results and Discussion

5.1 Motion Analysis

5.1.1 Repeatability. The repeatability of the stage's motion is critical to the function of the tool. To evaluate the repeatability of the stage, a series of measurements spanning hours or days were performed. The targets of the measurements were a double-side-polished silicon wafer and a ASME grade 0 ceramic gage block. The height measurement of the laser distance sensor was aligned with the position of the tool along its axis of motion by the linear encoder. Figure 6 shows the error compared to the mean of a continuous set of 25 measurements of the silicon wafer over four hours while the tool was moving at 5 mm/min. The mean error of the measurements was $0.18\,\mu$m with a 95% confidence interval of $0.03-0.33\,\mu$m which demonstrates a high repeatability that is suitable for this application.

To further test the repeatability, the same scan was taken three days apart. The individual scans are compared in Fig. 7. The repeatability remained acceptable, but the measurement's profile does not match the flatness expected from a prime grade silicon wafer or gage block. The visible $\sim 5\,\mu$m variation in the measurement signal can be attributed to the repeatable error in the tool motion. However, this repeatable error can be compensated for in the motion control system.

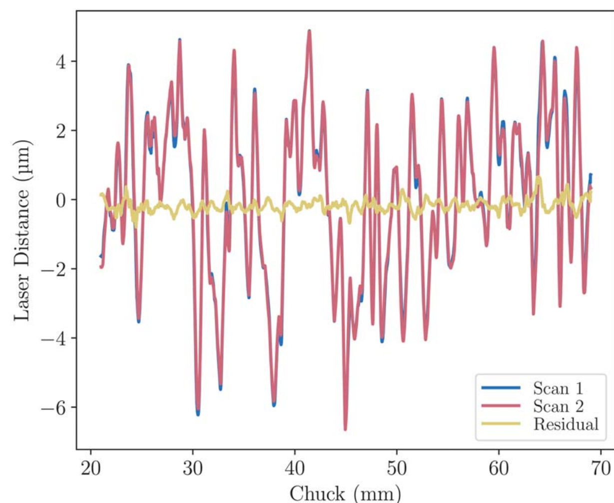

Fig. 7 Comparison of individual scans taken three days apart showing good agreement, but large repeatable error motion. Residual mean: $0.26\,\mu$m.

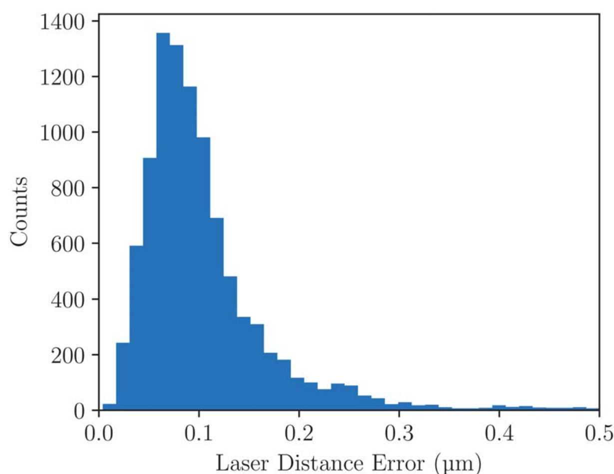

Fig. 6 Error from mean for each stage position for 25 continuous wafer scans over four hours. Mean: $0.18\,\mu$m, 95% confidence interval: $0.03-0.33\,\mu$m.

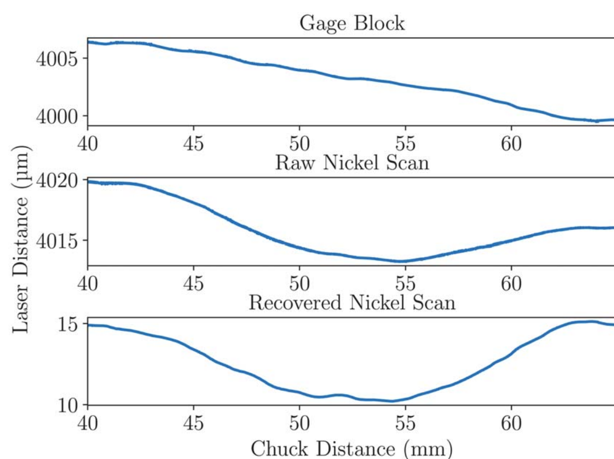

Fig. 8 Measurements demonstrating the removal of repeatable error by subtracting a ground truth measurement from a nickel sample measurement

Downloaded from http://asmedigitalcollection.asme.org/manufacturingscience/article-pdf/145/2/024501/6919480/manu_145_2_024501.pdf?casa_token=Rj5vsSdcsGUAAAAA:VzmV6JDaYR6fdRjDFGw7A4JUq2PUpl6WlFnVsUSqRbvklgI7lhOhvFSrhBdRF2DSElSKcgU by University of Texas At Austin user on 07 S

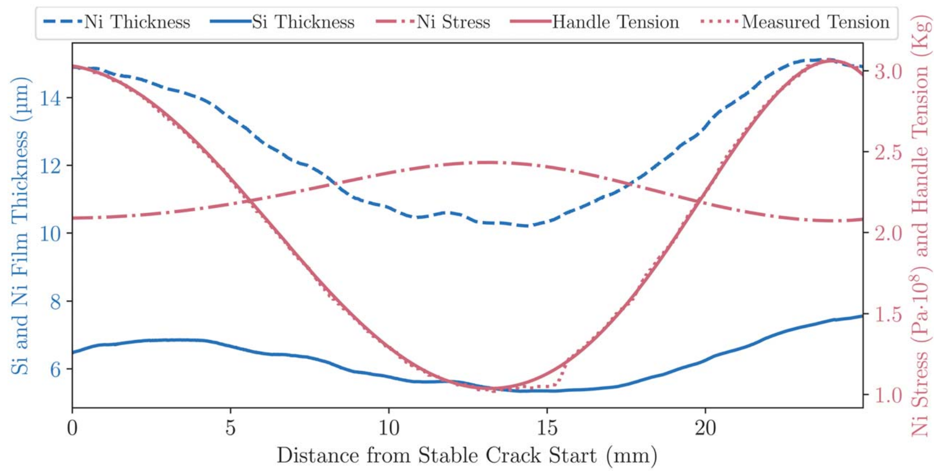

Fig. 9 Wafer profile measurement demonstrating load compensation and thickness control. Silicon and nickel thickness profiles are shown on the left axis and nickel stress and handle film tension on the right.

5.1.2 Remove Repeatable Error by Gage Block. Without another method of canceling repeatable error, a ASME grade 0 white ceramic gage block was used as a ground truth. It is flat to within 40 nm and an ideal laser target. Several scans of the gage block were taken before each wafer measurement and the gage profile was subtracted from the wafer profile. Unfortunately, this method limited the measurement range to the length of the available gage block, which was 30 mm (Fig. 8).

5.2 Load Compensation and Uniformity. After confirming the metrology capabilities of the tool, a demonstration of load compensation was performed. A typical exfoliation sample was prepared with a (100) prime grade double-side-polished silicon wafer and approximately 13 μm of electroplated nickel. The sample was then heat treated at 230°C for 30 min and exfoliated on the tool using a compensated load profile targeting a uniform silicon film thickness of 4 μm. Measurements were taken throughout to produce the profiles seen in Fig. 9 and an image of the film is shown in Fig. 10. The measured silicon and nickel film thicknesses are on the left axis. The right axis gives the loading in the form of both the handle tension and nickel stress as context.

Fig. 10 Image of silicon film sample corresponding to Fig. 9

The resulting silicon film is thicker than 4 μm, but appears to have reduced dependence on the variations in the inputs. To quantify the result, the standard deviation of the silicon profile is compared with that from Fig. 4. To further describe the decoupling of the silicon from the nickel, a "uniformity ratio" is suggested, where the standard deviation of the silicon is divided by the standard deviation of the nickel. The results of these metrics are shown in Table 1, where both show significant improvement with 53% better uniformity and 92% improvement in the uniformity ratio.

To compare the measured compensated film thickness with what would have been produced without compensation, the model was reconfigured to compute the estimated silicon film thickness from the measured inputs and an uncompensated handle tension. Figure 11 compares the measured profile from Fig. 9 with the model predicted result for a constant 1 N handle tension. The result shows improved uniformity and reduced thickness, but also that the model has over-estimated the compensated load's effect at higher nickel thicknesses. With some tuning of the model and metrology, a nearly constant film thickness should be achievable.

Figure 12 is surface visualization comparing a wafer exfoliated on the previous tool compared to the new one. The surface was generated using a combination of line scans using a confocal microscope and differential laser distance point measurements with basic interpolation between to aid visualization of the surface. The surface created by the new tool shows improved average uniformity and lower thickness. The magnitude of the linear trend in thickness across the wafer has also been reduced, but not completely eliminated. This is due to the fact that the active compensation is limited to the axis of exfoliation (y) and the non-uniform loading remains in the opposite axis (x).

Table 1 Silicon uniformity results comparing the new tool with active compensation to the old prototype

	σ_{Si} (μm)	σ_{Si}/σ_{Ni}
Without compensation	1.37	4.39
With compensation	0.65	0.37
% Improvement	53%	92%

...m http://asmedigitalcollection.asme.org/manufacturingscience/article-pdf/145/2/024501/6919480/manu_145_2_024501.pdf?casa_token=Rj5vsSdcsGUAAAAA:VzmV6JDaYR6fdRjDFGw7A4JUq2PUpl6WlFnVsUSqRbvklgl7lhOhvFSrhBdRF2DSElSKcgU by University of Texas At Austin user on 07 S...

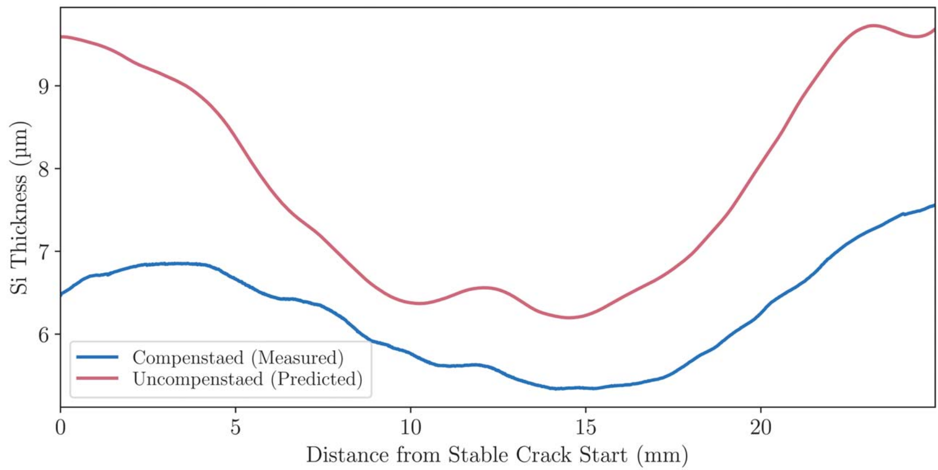

Fig. 11 Comparison of predicted uncompensated exfoliated film and measured compensated film

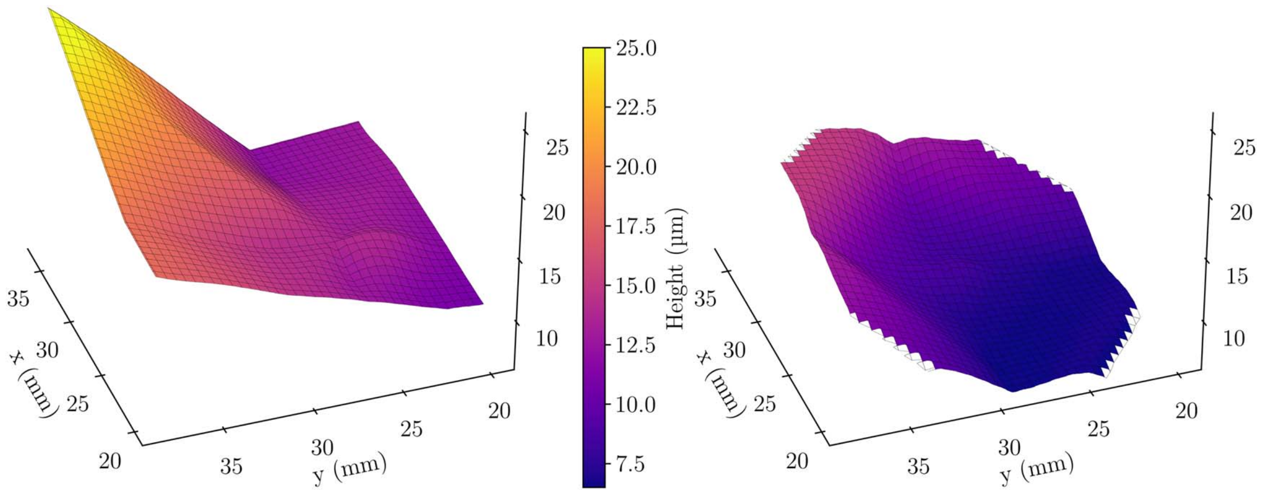

Fig. 12 Comparison of 3D visualization of a uncompensated wafer surface (left) from the initial prototype tool and compensated surface (right) from the new proactive precision tool (exfoliated along the *y* axis)

Table 2 Roughness averages and one standard deviation for ten measurements of a 4.2 mm^2 area for wafers exfoliated with the wedge-type tool, hand peeled with tape, controlled peeling tool, and new tool. The wafers were exfoliated along the *x* axis

	Wedge tool	Hand peel	Roller tool	New tool
S_a (nm)	151.0 ± 21.0	107.0 ± 150.0	75.5 ± 21.0	25.1 ± 7.0
S_z (μm)	3.46 ± 0.50	1.99 ± 1.70	1.15 ± 0.80	0.22 ± 0.05

5.3 Roughness. The roughness of the rigid wafer after exfoliating the flexible layer was measured using white light interferometry (Veeco Wyko NT-1000). It can be used as a metric to differentiate between the different exfoliation approaches. Ten measurements of a 4.2 mm^2 area distributed over the wafer were taken for the samples exfoliated using the wedge tool, hand peel, roller tool, and precision tool. A quantitative comparison of the roughness parameters, S_a (arithmetic mean height) and S_z (difference between roughness peak and valley) is presented in Table 2 and a qualitative comparison of the roughness can be seen in Fig. 13. As seen in Table 2, the surface roughness measured using the wedge tool and hand peeling approach is significantly 5.0× and 3.3× higher than the controlled exfoliation tool presented in this paper. The active compensation in the new tool improved the surface roughness by 67% as compared to previous roller tool without any compensation. Figure 13 shows a smoother surface finish along the exfoliation direction for the precision tool as compared to the wedge tool, hand peel, and roller tool approaches.

Downloaded from http://asmedigitalcollection.asme.org/manufacturingscience/article-pdf/145/2/024501/6919480/manu_145_2_024501.pdf?casa_token=Rj5vsSdcsGUAAAAA:VzmV6JDaYR6fdRjDFGw7A4JUq2PUpl6WlFnVsUSqRbvkIg7lhOhvFSrhBdRF2DSElSKcgU by University of Texas At Austin user on 07 S

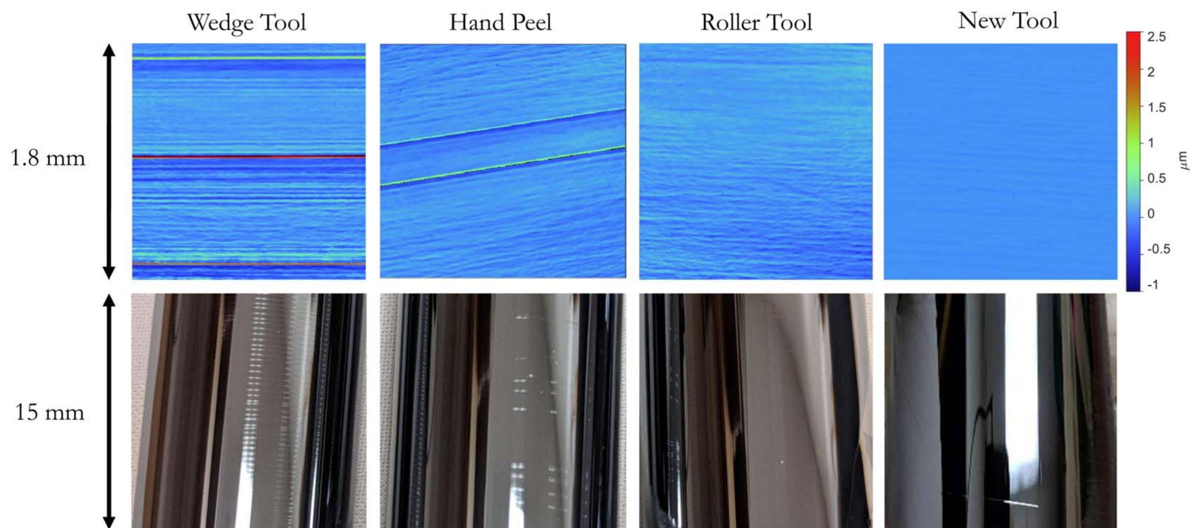

Fig. 13 Roughness comparison: (top) white light interferometer measurements of each method, (bottom) photographs of each sample. Note regular ridges on the wedge tool sample and irregular ridges on the hand peeled sample.

6 Conclusion

The advent of high-throughput semiconductor processing techniques has opened up a demand for the microscale flexible electronics for applications in the biosensors, health diagnostics, soft robotics, and structural health monitoring. Conventional lithographic approaches provide the lowest barrier to entry for reliably fabricating these flexible microelectronics on silicon. However, there is a need to transition into reliably producing these silicon flexible substrates. Wafer-scale exfoliation of silicon can be done by controlled brittle fracture. However, the uncontrollable nature of the exfoliation methods presented in previous works affects the uniformity, repeatability, and production scale adaptability of this process. Though further experiments are required to prove performance at scale, we have shown in this paper that improvements in the approach for controlled exfoliation of monocrystalline silicon films can produce high quality, uniform silicon thin films. The updated design of the exfoliation tool reduced unwanted motion and improved the exfoliated wafer surface uniformity and roughness. The addition of active compensation of the handle layer improved the uniformity of the exfoliated silicon film and provides a lever for tuning the process at scale. Further improvements to this tool can be made by developing a reliable tensile layer material and improving the deposition methods.

Conflict of Interest

There are no conflicts of interest.

Data Availability Statement

The datasets generated and supporting the findings of this article are obtainable from the corresponding author upon reasonable request.

References

[1] Gu, Y., Zhang, T., Chen, H., Wang, F., Pu, Y., Gao, C., and Li, S., 2019, “Mini Review on Flexible and Wearable Electronics for Monitoring Human Health Information,” Nanoscale Res. Lett., **14**(1), p. 263.

[2] Ying, M., Bonifas, A. P., Lu, N., Su, Y., Li, R., Cheng, H., Ameen, A., Huang, Y., and Rogers, J. A., 2012, “Silicon Nanomembranes for Fingertip Electronics,” Nanotechnology, **23**(34), p. 344004.

[3] Kim, J., Lee, M., Shim, H. J., Ghaffari, R., Cho, H. R., Son, D., Jung, Y. H., Soh, M., Choi, C., Jung, S., Chu, K., Jeon, D., Lee, S.-T., Kim, J. H., Choi, S. H., Hyeon, T., and Kim, D.-H., 2014, “Stretchable Silicon Nanoribbon Electronics for Skin Prosthesis,” Nat. Commun., **5**(5747).

[4] Ha, M.-H., Choi, J.-K., Park, B.-M., and Han, K.-Y., 2021, “Highly Flexible Cover Window Using Ultra-thin Glass for Foldable Displays,” J. Mech. Sci. Technol., **35**(2), pp. 661–668.

[5] Kireev, D., Seyock, S., Ernst, M., Maybeck, V., Wolfrum, B., and Offenhäusser, A., 2016, “Versatile Flexible Graphene Multielectrode Arrays,” Biosensors, **7**(4), p. 1.

[6] Yoon, J., Cho, H.-Y., Shin, M., Choi, H. K., Lee, T., and Choi, J.-W., 2020, “Flexible Electrochemical Biosensors for Healthcare Monitoring,” J. Mater. Chem. B, **8**(33), pp. 7303–7318.

[7] Park, H., Lee, Y., Kim, N., Seo, D., Go, G., and Lee, T., 2020, “Flexible Neuromorphic Electronics for Computing, Soft Robotics, and Neuroprosthetics,” Adv. Mater., **32**(15), p. 1903558.

[8] Kim, T. S., Kim, H. J., Geum, D.-M., Han, J.-H., Kim, I. S., Hong, N., Ryu, G. H., Kang, J., Choi, W. J., and Yu, K. J., 2021, “Ultra-Lightweight, Flexible InGaP/GaAs Tandem Solar Cells With a Dual-Function Encapsulation Layer,” ACS Appl. Mater. Interfaces, **13**(11), pp. 13248–13253.

[9] Pudasaini, P. R., Sharma, M., Ruiz-Zepeda, F., and Ayon, A. A., 2014, “Ultrathin, Flexible, Hybrid Solar Cells in Sub-Ten Micrometers Single Crystal Silicon Membrane,” 2014 IEEE 40th Photovoltaic Specialist Conference (PVSC), Denver, CO, June 8–13, IEEE Silver Spring, MD, pp. 0953–0955.

[10] Ahn, J., Chou, H., and Banerjee, S. K., 2017, “Graphene-Al_2O_3-silicon Heterojunction Solar Cells on Flexible Silicon Substrates,” J. Appl. Phys., **121**(16), p. 163105.

[11] Pagliaro, M., Ciriminna, R., and Palmisano, G., 2008, “Flexible Solar Cells,” ChemSusChem, **1**(11), pp. 880–891.

[12] Laflamme, S., Kollosche, M., Connor, J. J., and Kofod, G., 2013, “Robust Flexible Capacitive Surface Sensor for Structural Health Monitoring Applications,” J. Eng. Mech., **139**(7), pp. 879–885.

[13] Huang, S., Liu, Y., Zhao, Y., Ren, Z., and Guo, C. F., 2019, “Flexible Electronics: Stretchable Electrodes and Their Future,” Adv. Funct. Mater., **29**(6), p. 1805924.

[14] Corzo, D., Tostado-Blázquez, G., and Baran, D., 2020, “Flexible Electronics: Status, Challenges and Opportunities,” Front. Electron., **1**, p. 594003.

[15] Banerjee, G., and Rhoades, R. L., 2019, “Chemical Mechanical Planarization Historical Review and Future Direction,” ECS Trans., **13**(4), pp. 1–19.

[16] Williams, J. S., 1998, “Ion Implantation of Semiconductors,” Mater. Sci. Eng. A., **253**(1-2), pp. 8–15.

[17] Bedell, S. W., Fogel, K., Lauro, P., Shahrjerdi, D., Ott, J. A., and Sadana, D., 2013, “Layer Transfer by Controlled Spalling,” J. Phys. D: Appl. Phys., **46**(15), p. 152002.

[18] Kashyap, K., Lai, D.-Y., Zheng, L.-C., Hou, M. T., and Yeh, J. A., 2015, “Rollable Silicon IC Wafers Achieved by Backside Nanotexturing,” IEEE Electron. Device Lett., **36**(8), pp. 829–831.

[19] Thouless, M. D., Evans, A. G., Ashby, M. F., and Hutchinson, J. W., 1987, “The Edge Cracking and Spalling of Brittle Plates,” Acta. Metall., **35**(6), pp. 1333–1341.

[20] Hensen, J., Niepelt, R., Kajari-Schroder, S., and Brendel, R., 2015, “Directional Heating and Cooling for Controlled Spalling,” IEEE J. Photovoltaics, **5**(1), pp. 195–201.

[21] Zhai, Y., Mathew, L., Rao, R., Xu, D., and Banerjee, S. K., 2012, “High-Performance Flexible Thin-Film Transistors Exfoliated From Bulk Wafer,” Nano Lett., **12**(11), pp. 5609–5615.

[22] Bedell, S. W., Shahrjerdi, D., Hekmatshoar, B., Fogel, K., Lauro, P. A., Ott, J. A., Sosa, N., and Sadana, D., 2012, “Kerf-Less Removal of Si, Ge, and III–V Layers by Controlled Spalling to Enable Low-Cost PV Technologies,” IEEE J. Photovoltaics, **2**(2), pp. 141–147.

om http://asmedigitalcollection.asme.org/manufacturingscience/article-pdf/145/2/024501/6919480/manu_145_2_024501.pdf?casa_token=Rj5vsSdcsGUAAAAA:VzmV6JDaYR6fdRjDFGw7A4JUq2PUpl6WlFnVsUSqRbvklgI7lhOhvFSrhBdRF2DSEISKcgU by University of Texas At Austin user on 07 S

[23] Ward, M., and Cullinan, M., 2019, "Design of Tool for Exfoliation of Monocrystalline Microscale Silicon Films," ASME J. Micro Nano-Manufacturing, **7**(1), p. 011003.
[24] Ward, M., and Cullinan, M., 2019, "A Fracture Model for Exfoliation of Thin Silicon Films," Int. J. Fract., **216**, pp. 161–171.
[25] Pedregosa, F., Varoquaux, G., Gramfort, A., Michel, V., Thirion, B., Grisel, O., Blondel, M., Prettenhofer, P., Weiss, R., Dubourg, V., Vanderplas, J., Passos, A., Cournapeau, D., Brucher, M., Perrot, M., and Duchesnay, E., 2011, "Scikit-Learn: Machine Learning in Python," J. Mach Learning Res., **12**, pp. 2825–2830.
[26] Buitinck, L., Louppe, G., Blondel, M., Pedregosa, F., Mueller, A., Grisel, O., Niculae, V., Prettenhofer, P., Gramfort, A., Grobler, J., Layton, R., Vanderplas, J., Joly, A., Holt, B., and Varoquaux, G., 2013, "API Design for Machine Learning Software: Experiences From the Scikit-Learn Project," arXiv: 1309.0238.
[27] "UT-NDML Si-Exfo," Original-date: 2020-08-08T21:07:43Z. 2022-02-03, https://github.com/UT-NDML/Si-Exfo. Accessed March 2, 2022.
[28] Ward, M., 2018, "Wafer Scale Exfoliation of Monocrystalline Micro-Scale Silicon Films," Thesis, https://repositories.lib.utexas.edu/handle/2152/69093, Accessed November 13, 2018.

Downloaded from http://asmedigitalcollection.asme.org/manufacturingscience/article-pdf/145/2/024501/6919480/manu_145_2_024501.pdf?casa_token=Rj5vsSdcsGUAAAAA:VzmV6JDaYR6fdRjDFGw7A4JUq2PUpl6WlFnVsUSqRbvklgI7lhOhvFSrhBdRF2DSEISKcgU by University of Texas At Austin user on 07 S